To be published in Applied Optics:

Title:	Rapid, Automated Measurement of Layer Thicknesses on Steel Coin Blanks Using LIBS Depth-Profiling
Authors:	George Asimellis, Aggelos Giannoudakos, and Michael Kompitsas
Accepted:	1 November 2006
Posted:	6 November 2006
Doc. ID:	72423

Rapid, Automated Measurement of Layer Thicknesses on Steel Coin Blanks Using LIBS Depth-Profiling

George Asimellis[1*], Aggelos Giannoudakos[2,3], Michael Kompitsas[3]

1 Faculty of Physics, Aristotle University of Thessaloniki, Thessaloniki 54124, Greece

* Corresponding author. Email address: gasim@auth.gr

2 School of Chemical Engineering, National Technical University of Athens, 9, Iroon Polytechniou Str., Zografou, 15780 Athens, Greece

3 National Hellenic Research Foundation, Theoretical and Physical Chemistry Institute, 48 Vasileos Konstantinou Ave., 11635 Athens, Greece

Abstract

We report application of a near-real time method to determine layer thickness on electroplated coin blanks. The method was developed on a simple Laser-Induced-Breakdown Spectroscopy (LIBS) arrangement by monitoring relative emission line intensities from key probe elements via successive laser ablation shots. This is a unique LIBS application where no other current spectroscopic method (ICP or XRF) can be applied effectively. Method development is discussed, and results with pre-calibrated coins are presented.

OCIS codes: 120.0120, 120.6200 , 140.3440, 300.6360, 350.3390

Introduction

The Royal Canadian Mint (RCM) plating facility in Winnipeg, Canada, has identified a problem with performing Quality Control of their electroplated coin blanks. Typically, coins, of a ferritic steel core, are electro-plated with three (3) layers, two (2) layers of approximately 4-8 μm-thick nickel, separated with a middle layer of 7-10 μm thick copper. A rapid and automated technique was sought to perform near real-time quality assurance on production coin blanks to replace current methods of coin sectioning and subsequent optical metallographic measurements, because these mechanical methods are slow and labor intensive.

Laser-Induced Breakdown Spectroscopy (LIBS) enables multi-elemental identification and quantitative analysis requiring little or no sample preparation. A schematic of LIBS arrangement is shown in Figure 1. A high-power laser pulse is focused just above or below the sample surface, creating a localized area of material removal (less than 1 *mm* -wide and sub-μm deep per shot). Particles from the ablated material are subsequently ionized and thus a hot plasma is created. Upon plasma cooling ions recombine, and consequent excited atoms relax, radiating atomic emission lines, characteristic of the ablated sample constituent elements. By spectrally examining the optical emission it is possible to identify the ablated area's atomic composition. This is achieved by a high-resolution spectrograph, on which the optical plasma radiation is directed, by means of fused-silica optics and steering mirrors. The spectrum is recorded on a gated, intensified CCD detector. Thus, specific quantitative element analysis can be accomplished in near real time [1-3].

This work is focusing on the applicability of LIBS for rapid identification of plated layer thickness. The elemental composition of the ablated layer can be analyzed for every successive shot as the laser penetrates deeper into the material at a repeatable rate. Thus the number of shots required to penetrate a specific layer can be determined by monitoring the appearance of new probe elemental

lines or the sharp decline/increase in the line intensities (photon count) of existing elemental lines. Thus LIBS can provide detailed knowledge of the layered depth profile on a very localized sample area, less than 1 *mm*-wide [4-13]. It is this characteristic depth-profiling capability of LIBS that provided motivation for this work.

An analytical technique for trace element analysis that has been applied to coin analysis[14] is Energy-Dispersive X-Ray Fluorescence (EDXRF). Compared to this technique, LIBS is advantageous in the aspect of being able to detect all elements, independent of their atomic number, and, more important, can provide a detailed information of elemental constitution of each (sub-μm) ablation layer. In addition, because the area of the ablation crater is in the vicinity of 1 mm^2, detailed depth-profiling analysis is possible.

For this development a simple laboratory LIBS setup was used (figure 1) using a fundamental Nd:YAG laser (YG 981, Quantel, France) with pulse energy 30 *mJ* and pulse duration of 7 *ns*, conventional laser optics delivery to the target and plasma optical emission collection, a Czerny-Turner (HRP, Jobin-Yvon, Edison, NJ, USA) spectrometer fitted with 2,400 *lines/mm* holographic grating. A gated intensified CCD camera (GEN II, Andor Technologies, Belfast, UK) with 15% quantum efficiency (average) was used for optical signal detection.

Coin samples were placed on a servo-controlled positioning stage. The programmable stage can position the sample on the desired location relative to the incident laser beam with μm precision, allowing the desired number of shots at each spot and then moves to the next spot or next coin.

Method Development

As shown in Figure 2, the electroplated coins were composed of three layers superimposed on a ferritic steel core. From bottom to top, interface C separates the steel core from the lower Ni layer (identified as #1), of approximate thickness of 5 μm. This layer is separated by interface B from a Cu layer

(identified as #2), of approximate thickness of 7 μm. Interface A separates the Cu layer from the top Ni layer (identified as #3), of approximate thickness of 4 μm. Thus the first layer to be 'identified' by the method was layer #3.

Selection of suitable atomic emission lines from all three elements of interest (Cu, Ni, and Fe) was the first step in the process. These probe lines must be associated only with the presence of the element in question in order to be used in determining its presence/absence. In addition, data from each ablation layer must simultaneously determine the presence/absence and relative intensity of probe lines from all three elements. Thus it was mandatory that suitable emission lines from all three elements of interest must exist in the same spectral window, which had a typical width of 15-20 *nm*, depending on the central wavelength[15].

The following lines of interest satisfying the above criteria were identified and selected: Cu 324.7 *nm*, 327.4 *nm*, and 330.8 *nm*, Ni 338.1 *nm*, 342.4 *nm*, and 352.9 *nm*, and Fe 358.1 *nm*. As shown in Figure 3, for each line, peak intensity was measured from top to the specific spectral baseline.

The next step in method development involved experimental determination of the optimal parameters that provided interference-free peaks with adequate signal-to-baseline ratio. These parameters included gate delay (time duration, in μs, between laser firing and start of emission detection) and gate width (time duration, in μs, for emission detection). Other parameters that affected precision and analysis time, such as laser pulse energy, shot repetition rate, laser focus, etc, were also optimized experimentally[16]. For example, shot repetition rate was selected at 2 *Hz*, because this setting appeared to give the best combination of speed and precision.

During successive shots, as the layer penetration depth increased, neither all of these lines were present, nor were their relative intensity exactly as shown in Figure 3. While transitioning, for

example, from the top Ni to the Cu layer, the Cu lines intensity (photon counts) increased substantially. Similarly, early shots produced no Fe peak at all. The first appearance of the Fe peak was considered as an indicator that ablation has reached the iron core. Even in the absence of calibration standards, by simply counting the number of shots required for these changes to appear, a semi-quantitative indication of layer thickness was possible.

Results and Discussion

Figure 4 shows the evolution of the line intensities (photon counts) of three selected peaks (324.7 *nm* for Cu, 338.1 *nm* for Ni, and 358.1 *nm* for Fe) for increasing shot sequence. The following qualitative observations can be made:

Until laser shot number count 75, it is clear that the origin of the ablated material was layer #3, the top nickel layer. The Ni 338.1 line intensity is constantly high until shot #100 and the Cu 324.7 line intensity is low until shot # 75. Time required to reach this Ni-Cu interface A was approximately 0.5 *min*. Between counts 75-250 it is observed that the Ni line intensity is decreasing constantly, while the Cu line intensity is increasing constantly until shot # 200. It is clear that the source of the ablated material was layer #2, the middle copper layer. Time to reach this interface B from the surface was less than 2 *min*. Between counts 250-400 it appears that ablation material originates from layer #1, the lower nickel layer, since the Ni 338.1 line has a constant photon count increase. The first indication of the Fe 358.1 *nm* line was considered as an indication that ablation had reached interface C, separating the Ni layer #1 from the Fe base. Given that the laser shots were fired at 2 *Hz*, it is derived that less than 3.5 *min* were required to identify this last interface C.

One might have expected an immediate disappearance of the nickel line for the succeeding shots; this, however was not observed because the ablated material emanates not only from the crater bottom, but also from side walls and, partially, from previously-ablated melted material (e.g. for layer

#3) that was partially re-deposited in the pit. In other words, material is not only ablated from the crater base but also from the crater walls, which, as penetration depth increased to many μm, had an increasing contribution to the ablated material.

This effect was a result of the relative large pulse duration (7 *ns*) relative to the material's thermal constant effect, and the cross-section laser beam being Gaussian[10, 17-18]. The resulting crater shape was somehow irregular, as it is demonstrated in Figures 5, where study pictures from Cu and Ni craters formed from a 30 *mJ* Nd:YAG fundamental pulse are shown.

In general, transitions involving a newly-encountered element, e.g. from Ni to the Cu layer can be identified with quite ease. However, when a subsequent layer consists of an element having already been encountered previously, (e.g. the Ni # 1 layer) identification of the transition is not obvious.

The objectives of the subsequent development work were to :

- Develop a method to quantify layer depths by establishing quantitative criteria
- Establish measurement precision
- Determine technique accuracy, and
- Compare with unknown samples to verify validity

Because for each layer thickness varied from center to edge due to the electro-deposition technique, method repeatability and precision was studied by shooting a specific test coin at eight different spots along a semicircle, having constant radius (3 *mm*) from the coin center. The craters, about 1 mm^2 wide, were approximately 2.5 *mm* apart. The objective was to test the consistency of the respective probe line intensity pattern. In Figure 6, the consistency of the Fe 358.1 *nm* line is shown for eight different spots. Similarly, in Figure 7, and Figure 8, the consistency of the Ni 338.1 *nm* line and of the Cu 324.7 *nm* lines are shown. Having established that a consistent pattern appears in all expected layer interfaces, we proceeded to identify the quantitative criteria that enable a qualitative

observation into a measured thickness value with adequate precision and in a reproducible manner, as follows:

Interface A, transition from top Ni layer #3 to middle Cu layer #2.

While in the top Ni layer, the Cu 324.7 *nm* peak appeared to have a near-constant, minimum intensity (Figures 4 and 8). Upon reaching interface A, the Cu line intensity increases distinctively. Therefore, the first step in the process was to estimate the mean value of the Cu peak intensity in the vicinity of this minimum (i.e., between shots 20 and 40, as the first 10 shots can be considered 'cleaning shots'). This minimum Cu peak intensity value is subsequently called baseline. To ensure that transition through interface A was identified, a definite increase must be determined in the Cu peak intensity: the Cu peak intensity had to exceed a certain threshold with respect to the baseline. Following this, the shot number by which the Cu peak intensity exceeded the threshold was identified. Several threshold values were considered, ranging from +10% to +400%, with respect to the background. For example, a threshold of 1.10 indicates that the Cu peak intensity exceeded the baseline by +10%, and a threshold of 2.50 indicates that the Cu peak intensity exceeded the baseline by +150%. In addition, various line intensity data smoothing (or moving average windows) from 3 to 9 points (data = line intensities of successive shots) were considered. The values for these parameters (threshold and smoothing) that provided a stable criterion for layer thickness determination were systematically investigated.

Table 1 summarizes the repeatability statistics on the Cu 324.7 *nm* line based on the method described above. Column 1 indicates the chosen threshold value, column 2 indicates the average shot number (with 7 point data smoothing), at which the Cu 324.7 *nm* line intensity exceeds the threshold, and in column 3, is the relative standard deviation (RSD) from all eight ablation spots, which were expected to have the same layer thickness.

The results in table 1 indicate that the Cu peak arrays have a 5% to 6% RSD precision, largely insensitive to the chosen value for threshold. Similar results were produced when smoothing of 3, 5, and 9 points were chosen. Comparing the results from table 1 and raw data in figure 8, we selected a criterion of threshold value of 1.30, translating to 30% above the Cu 324.7 *nm* baseline and a moving average of 7 data points.

Interface B, transition from middle Cu layer # 2 to the lower Ni layer.

Inspection of Figures 4 and 7 indicates that interface B corresponds to a minimum value of the Ni peaks intensity, after which an increase for 200 shots is noted. It is also noted that the Cu line intensity appears to have a maximum, after which a consistent decrease occurs. Thus, it was decided to investigate the variation of the Cu-to-Ni line ratio intensity, as follows: Since three prominent Ni peaks were available, namely the Ni 338.1, 342.4 and 352.9 *nm* lines, the average of these three Ni lines was considered. This formed the Ni data array, while the Cu line array was formed from the Cu 324.7 *nm* line intensity data. The ratio of these data arrays for increasing laser shot number formed the Cu-to-Ni peak ratio. Such an array has a distinct maximum (see Figure 9a), corresponding to the transition from interface B. From the derivative of this array (Figure 9b), the shot number for which the derivative crosses zero indicates the transition corresponding to interface B.

Interface C, transition from the lower Ni layer to ferritic core

The method developed is similar to the one for interface A, using again baseline and threshold values, as defined in the corresponding section. Inspection of the Fe line intensity variation (Figures 4 and 6) suggests that until interface C is reached, the Fe 358.1 *nm* line intensity has a near-constant, minimum intensity. Upon reaching interface C, the Fe line intensity increases distinctively. Therefore, the first step in the process was to estimate the mean value of the Fe peak intensity in the vicinity of its

minimum (i.e., between shots 200 and 350). This minimum Fe peak intensity value is subsequently called Fe baseline. The objective was then to identify the shot with the Fe peak intensity meeting a specific threshold (indicating definite appearance of the Fe line). Having done this, the shot number for which the threshold is met, is determined. We investigated various threshold values ranging from +10% to +400%.

Table 2 summarizes the repeatability statistics on the Fe 358.1 *nm* line data based on the method described above for moving averages of 5 and 7 data points. Again, RSD is the relative standard deviation of the results obtained from all eight ablation spots, which are expected to have the same layer thickness. It is concluded that the method described above produces a 3% to 4% precision, largely independent of the threshold chosen. Similar results were produced when smoothing of 3 and 9 (not shown) were chosen. Comparing the results from Table 2 and raw data in Figure 6, we selected the criteria of threshold 4.0 (i.e. +300% above the Fe 358.1 baseline) and smoothing of 7 data points.

Calibrations

There were five (5) available coins (production standards), whose layer thickness was pre-measured on each side by RCM with an established method, conventional optical metallographic technique. The coins were cut in half with an approx. 2 *mm* kerf removed from the center, and subsequently edge-polished. These known thickness data are reported in Table 3. Each thickness, as given, carried a reading uncertainty of ± 1 μm, determined by the method's precision. This uncertainty is of particular concern in interface A, where it represents up to ± 25% relative uncertainty. This limitation impacts our ability to test our calibrations. Each calibration curve was assessed for linearity by the linear regression coefficient, R^2, computed by MS Excel.

Calibration on Interface A, transition from top Ni layer 3 to middle Cu layer 2.

Based on the technique described previously, calibration was performed on these coin standards. Selected parameters were threshold value of 1.30 (+30% of the Cu 324.7 baseline). The corresponding calibration curve is shown in figure 10. (Note: Two of the available standards were not usable for this calibration because of top layer contamination from prior runs).

The calibration has a linear regression coefficient of 0.75. Such a low-quality calibration curve does not yield significant confidence when used in determining layer thickness of unknown coins. Possible reasons for this poor calibration were the very limited dynamic range (4 to 6 μm) and the large relative error (± 1 μm) in the supplied standards known thickness.

Calibration on Interface B, transition from middle Cu layer 2 to lower Ni layer 3.

The corresponding calibration curve is shown in figure 11. The horizontal axis indicates the total thickness of the top Ni and Cu layers in μm. This calibration has a linear regression coefficient of 0.91, which is improved compared to the one yielded for interface A, and is expected to have a smaller error in determining unknown thickness. The relative reading error (± 1 μm in 12-16 μm readings) is much smaller compared to the relative error of interface A.

Calibration on Interface C, transition into the Fe core.

Selected parameters were threshold of 4.0 (+300% above the Fe 358.1 baseline) and smoothing of 5 data points. The corresponding calibration curve is shown in Figure 12. The horizontal axis is the total thickness of the upper Ni, middle Cu and lower Ni layers in μm. This calibration has a linear regression coefficient (R^2) of 0.98, which is now substantially improved than those yielded for the previous interfaces, because the relative reading error (± 1 μm, given by RCM) is now much smaller compared to the relative error of interfaces A and B.

Unknown coin thickness measurements based on calibrations.

Ten replicate coin blanks of unknown thickness were supplied by RCM for layer thickness measurement. On each coin surface, one point, at the center, was shot using the exact settings that produced the previously derived calibrations. Measurements for layer thickness of the unknown replicates are presented in Tables 4a, for interface A, Table 4b for interface B, and Table 4c for interface C. Method uncertainty is estimated based on each calibration's regression coefficient uncertainty ($1\text{-}R^2$), and on average was ± 0.1 μm. However, the pre-measured thicknesses used for comparison carried an uncertainty of ± 1 μm. The relative difference (in %) is also reported for each interface.

There is high relative difference in interface A thickness values, due to the relatively poor calibrations obtained with the supplied standards. However, the relative difference in interfaces B and C is drastically reduced. We believe calibrations and thus measurement accuracies for all interfaces can be improved significantly by using a greater number of more accurately known standard thickness and over a greater thickness range.

Conclusions

A LIBS application on determination of electroplated layer coating thickness on production coins has been demonstrated on a simple LIBS setup. This depth-resolution application on the multi-layer coin structure requires no sample preparation time. Thus, once the instrument is initially prepared, there is no further setup time for analysis, other than placing the samples in the holder. The principle of the technique is the correlation of elemental content analysis with ablation shot sequence. With the selected shot frequency of 2 *Hz*, to reach a total of 20-μm layer, the current analysis needs approximately 500 shots, or about four (4) minutes.

The developed analytical methods indicate a precision of 3%-6% over eight different ablation spots on a given sample. Calibrations, and thus improved accuracies, can be achieved with a greater number of more accurate standards over a larger dynamic range. In addition, modification of the laser beam profile (from Gaussian to flat front) to optimize crater configuration, will improve both accuracy and precision.

We believe that LIBS technology has a unique advantage in plated multi-layer thickness measurement and quality assurance, because it is rapid, simple, and can determine point-to-point variations in thickness over the plated/coated surface of interest.

Table Captions

1. Table 1: Layer transition identification results based on meeting a specific threshold above the Cu 324.7 *nm* baseline. See text for description.
2. Table 2: Layer transition identification results based on meeting a specific threshold above the Fe baseline. Average and RSD correspond to Fe 358.1 *nm* line intensity from all eight ablation spots.
3. Pre-measured layer thickness (in μm) of standard coins used in calibration.
4. Table 4a: Unknown coins layer interface A: calculations and comparison with known thickness. Method calculated thickness carries an uncertainty of $\pm$ 0.1 μm, while pre-measured thickness carries an uncertainty of $\pm$ 1 μm.

   Table 4b: Unknown coins layer interface B: calculations and comparison with known thickness.

   Table 4c: Unknown coins layer interface C: calculations and comparison with known thickness.

Figure Captions

1. Figure 1: Schematic of LIBS experimental setup.
2. Figure 2: Schematic of electroplated layers to be examined.
3. Figure 3: Selected probe emission lines obtained with a single spectral window. These are the Cu 324.7 *nm*, Cu 327.4 *nm*, Cu 330.8 *nm*, Ni 338.1 *nm*, Ni 342.4 *nm*, Ni 352.9 *nm*, and Fe 358.1 *nm*.
4. Figure 4: Evolution of the relative line intensities (appearing as photon counts) of three selected peaks (Cu 324.7 *nm*, Ni 338.1 *nm*, and Fe 358.1 *nm*) for increasing shot sequence.
5. Figure 5: Cu (top) and Ni (bottom) craters formed from a 40 *mW* Nd:YAG fundamental. The craters are about 1 mm^2 wide.
6. Figure 6: Consistency of the Fe 358.1 *nm* spectral line intensity for eight different spots along a semicircle, having constant radius (3 *mm*) from the coin center.
7. Figure 7: Consistency of the Ni 338.1 *nm* spectral line intensity for eight different spots along a semicircle, having constant radius (3 *mm*) from the coin center.
8. Figure 8: Consistency of the Cu 324.7 *nm* spectral line intensity for eight different spots along a semicircle, having constant radius (3 *mm*) from the coin center.
9. Figure 9: (a) Cu/Ni line intensity ratio and (b) Derivative. Zero crossing indicates transition from Cu to Ni.
10. Figure 10: Seven-point interface A (Ni-Cu) calibration curve.
11. Figure 11: Nine-point interface B (Cu-Ni) calibration curve.
12. Figure 12: Seven-point interface C calibration curve.

13. References

1. R. Sattmann, I. Monch, H. Krause, R. Noll, S. Couris, A. Hatziapostolou, A. Mavromanolakis, C. Fotakis, E. Larrauri, and R. Miguel, "Laser-induced breakdown spectroscopy for polymer identification," Appl. Spectrosc. **52**, 456-461 (1998).
2. M. Stepputat and R. Noll, "On-line detection of heavy metals and brominated flame retardants in technical polymers with laser-induced breakdown spectrometry," Appl. Opt. **42**, (30) 6210-6220 (2003).
3. S. Palanco and J. Laserna, "Full automation of a laser-induced breakdown spectrometer for quality assessment in the steel industry with sample handling, surface preparation and quantitative analysis capabilities," J. Anal. At. Spectrosc. **15**, (10) 1321-1327 (2000).
4. D.R. Anderson, C.W. McLeod, T. English, and A.T. Smith, "Depth Profile Studies Using Laser-Induced Plasma Emission Spectrometry," Appl. Spectrosc. **49**, (11) 691-701 (1995).
5. J.M. Vadillo and J.J. Laserna, "Depth-resolved analysis of multilayered samples by laser-induced breakdown spectrometry," J. Anal. At. Spectrosc. **12**, (8) 859-862 (1997).
6. L. St-Onge and M. Sabsabi, "Towards quantitative depth-profile analysis using laser-induced plasma spectroscopy: investigation of galvannealed coatings on steel," Spectrochim. Acta, Part B **55**, (3) 299-308 (2000).
7. V. Tornari, V. Zafiropulos, A. Bonarou, N.A. Vainos. and C. Fotakis, "Modern technology in artwork conservation: a laser-based approach for process control and evaluation," Opt. Laser Eng. **34**, (4-6) 309-326 (2000).
8. V. Margetic, M. Bolshov, A. Stockhaus, K. Niemax, and R. Hergenröder, "Depth profiling of multi-layer samples using femtosecond laser ablation," J. Anal. At. Spectrosc. **16**, (6) 616-621 (2001).

9. M.D. Mowery, R. Sing, J. Kirsch, A. Razaghi, S. Bechard, and R.A. Reed, "Rapid at-line analysis of coating thickness and uniformity on tablets using laser induced breakdown spectroscopy," J. Pharmaceut. Biomed. **28**, (5) 935-943 (2002).
10. D.G. Papazoglou, V. Papadakis, and D. Anglos, "In situ interferometric depth and topography monitoring in LIBS elemental profiling of multi-layer structures," J. Anal. At. Spectrosc. **19**, (4) 483-488 (2004).
11. P. Pouli, K. Melessanaki, A. Giakoumaki, V. Argyropoulos, and D. Anglos, "Measuring the thickness of protective coatings on historic metal objects using nanosecond and femtosecond laser induced breakdown spectroscopy depth," Spectrochim. Acta, Part B **60**, (7-8) 1163-1171 (2005).
12. M. Corsi, G. Cristoforetti, M. Giuffrida, M. Hidalgo, S. Legnaioli, L. Masotti, V. Palleschi, A. Salvetti, E. Tognoni, C. Vallebona, and A. Zanini, "Archaeometric analysis of ancient copper artefacts by laser-induced breakdown spectroscopy technique," Microchim. Acta **152**, (1-2) 105-111 (2005).
13. H. Balzer, St. Hölters, V. Sturm, and R. Noll, "Systematic line selection for online coating thickness measurements of galvanised sheet steel using LIBS," Anal. Bioanal. Chem. **385**, (2) 234–239 (2006).
14. N. Kallithrakas-Kontos, A.A. Katsanos, J. Touratsoglou, "Trace element analysis of Alexander the Great's silver tetradrachms minted in Macedonia," Nucl. Instr. and Meth. in Phys. Res. B **171**, 342-349 (2000).
15. G. Asimellis, A. Giannoudakos, and M. Kompitsas, "Accurate wavelength calibration in the Near-InfraRed for multielement analysis without the need of reference spectra," Appl. Optics, **45**, (35) (2006).

16. I. Bassiotis, A. Diamantopoulou, A. Giannoudakos, F. Roubani-Kalantzopoulou, and M. Kompitsas, “Effects of experimental parameters in quantitative analysis of steel alloy by laser-induced breakdown spectroscopy,” Spectrochim. Acta, Part B **56**, (6) 671-683 (2001).
17. V. Margetic, K. Niemax, and R. Hergenröder, “Application of femtosecond laser ablation time-of-flight mass spectrometry to in-depth multilayer analysis,” Analyt. Chem. **75**, (14) 3435-3439 (2003).
18. M. Corsi, G. Cristoforetti, M. Hidalgo, D. Iriarte, S. Legnaioli, V. Palleschi, A. Salvetti, and E. Tognoni, “Effect of laser-induced crater depth in laser-induced breakdown spectroscopy emission features,” Appl. Spectrosc. **59**, (7) 853-860 (2005).

TABLES

Table 1: Layer transition identification results based on meeting a specific threshold above the Cu 324.7 *nm* baseline. See text for description.

threshold	average	RSD
1.10	44	0.05
1.20	51	0.05
1.30	56	0.06
1.40	61	0.06
1.50	65	0.06
1.75	74	0.06
2.00	81	0.05
2.25	87	0.05
2.50	94	0.05

Table 2: Layer transition identification results based on meeting a specific threshold above the Fe baseline. Average and RSD correspond to Fe 358.1 *nm* line intensity from all eight ablation spots.

threshold	average	RSD	threshold	average	RSD
5-poing smoothing			*7-poing smoothing*		
1.10	402	0.03	1.10	402	0.03
1.50	410	0.04	1.50	410	0.04
2.00	412	0.04	2.00	413	0.04
2.50	415	0.04	2.50	416	0.03
3.00	418	0.03	3.00	418	0.03
3.50	420	0.03	3.50	419	0.03
4.00	422	0.03	4.00	422	0.03
4.50	422	0.03	4.50	424	0.03
5.00	426	0.04	5.00	426	0.04

Table 3: Known thickness data (in μm) of standard coins used in calibration. Each measurement carries a reading uncertainty of ± 1 μm.

coin sample	to interface A (upper Ni)	total to interface B (upper Ni and Cu)	total to interface C (upper Ni, Cu, and lower Ni)
1A	4	12	16
1B	5	15	20
2A	6	15	18
2B	5	13	16
3A	6	15	20
3B	4	13	18
4A	5	12	17
5A	4	13	17
5B	5	14	18

Table 4a: Unknown coins layer interface A: calculations and comparison with known thickness. Method calculated thickness carries an uncertainty of ± 0.1 μm, while pre-measured thickness carries an uncertainty of ± 1 μm.

sample	number of shots	method calculated thickness (μm)	pre-measured thickness (μm)	difference (%)
Q 31	59	4.9	4	-22.2
Q 32	105	9.9	8	-23.6
Q 33	78	7.0	8	13.1
Q 34	96	8.9	8	-11.3
Q 36	56	4.6	6	24.0
Q 37	73	6.4	7	8.4
Q 38	56	4.6	8	43.0

Table 4b: Unknown coins layer interface B: calculations and comparison with known thickness.

sample	number of shots	method calculated thickness (μm)	pre-measured thickness (μm)	difference (%)
Q 31	313	12.9	12	-7.4
Q 32	641	23.4	20	-17.0
Q 33	335	13.6	14	2.9
Q 34	383	15.1	14	-8.1
Q 36	402	15.7	16	1.6
Q 37	341	13.8	14	1.5
Q 38	615	22.6	18	-25.4

Table 4c: Unknown coins layer interface C: calculations and comparison with known thickness.

sample	number of shots	method calculated thickness (μm)	pre-measured thickness (μm)	difference (%)
Q 31	355	15.9	17	6.7
Q 32	598	23.4	23	-1.8
Q 33	366	16.2	18	10.0
Q 34	370	16.3	17	3.9
Q 36	467	19.3	20	3.3
Q 37	389	16.9	17	0.5
Q 38	604	23.6	23	-2.6

FIGURES

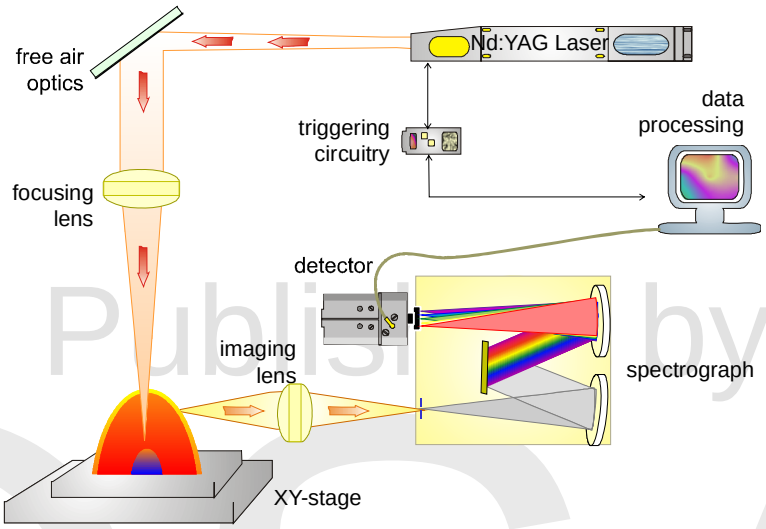

Figure 1 Schematic of LIBS experimental setup.

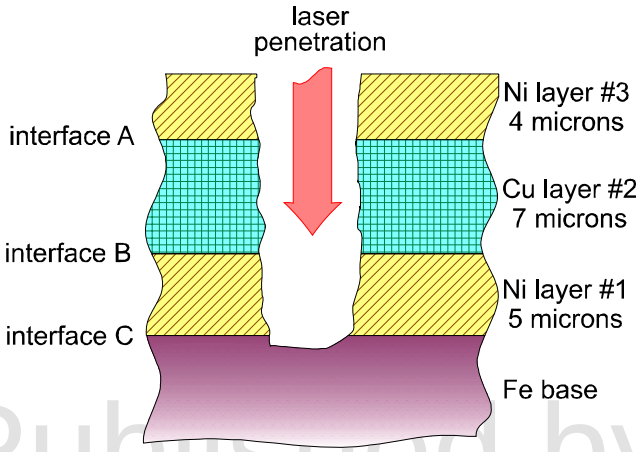

Figure 2: Schematic of electroplated layers to be examined.

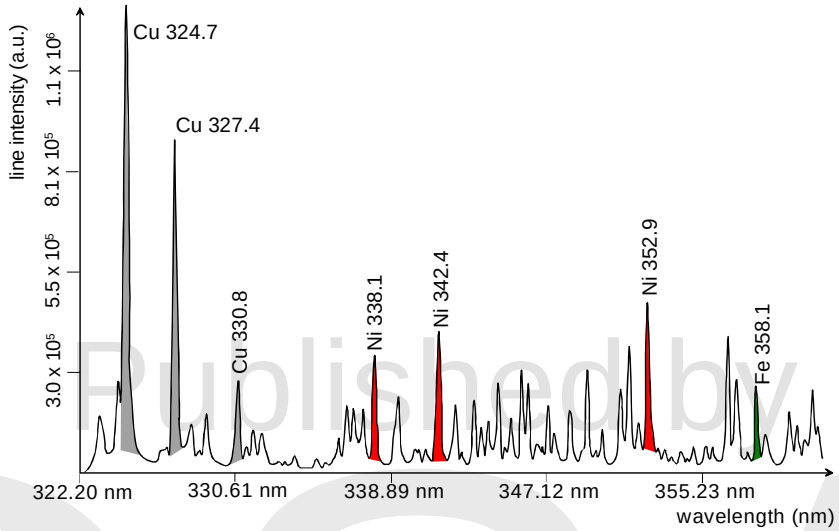

Figure 3: Selected probe emission lines obtained within a single spectral window. These are the Cu 324.7 *nm*, Cu 327.4 *nm*, Cu 330.8 *nm*, Ni 338.1 *nm*, Ni 342.4 *nm*, Ni 352.9 *nm*, and Fe 358.1 *nm*.

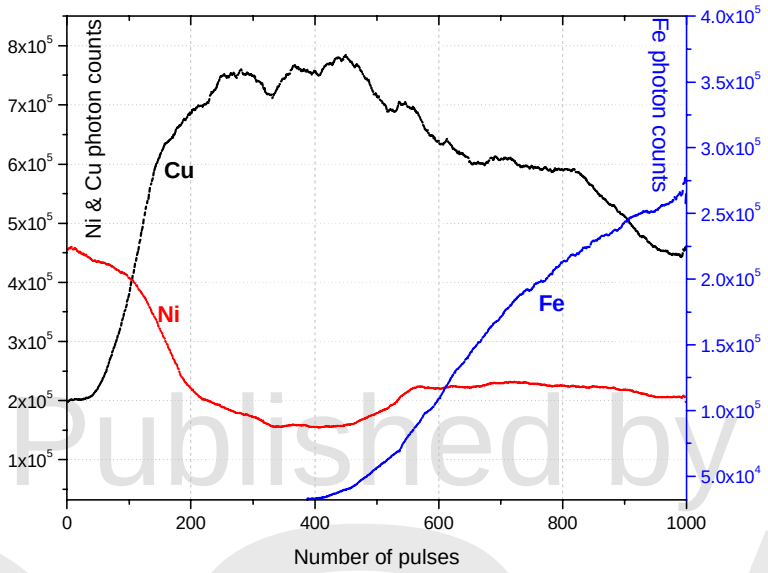

Figure 4: Evolution of the relative line strengths (appearing as photon counts) of three selected peaks (324.7 *nm* Cu, 338.1 *nm* Ni, and 358.1 *nm* Fe) for increasing shot sequence.

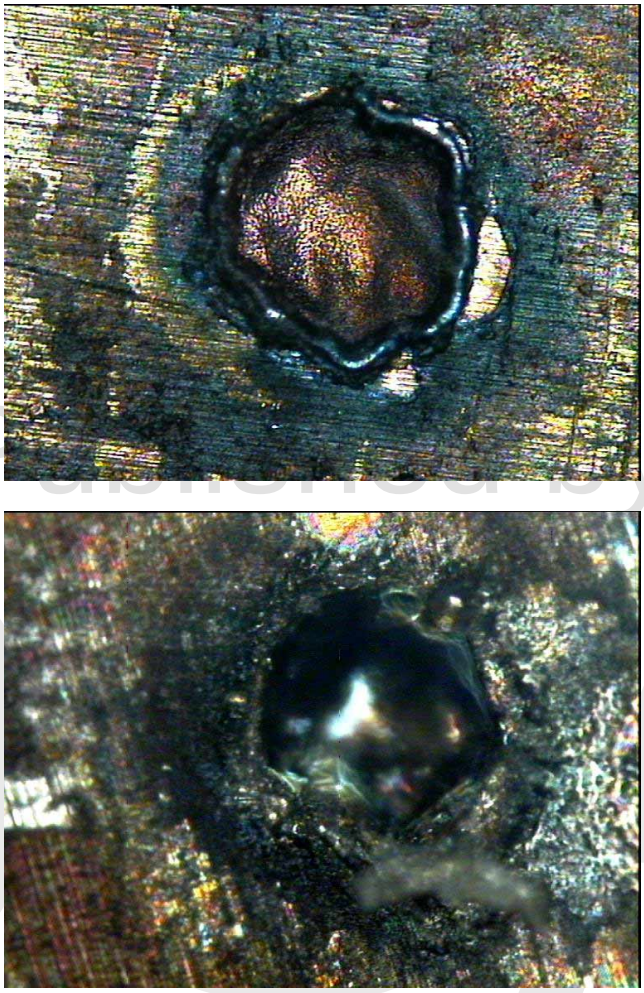

Figure 5: Cu (top) and Ni (bottom) craters formed from a 30 *mJ* Nd:YAG fundamental laser pulse. The crater area is approx. 1 mm^2 .

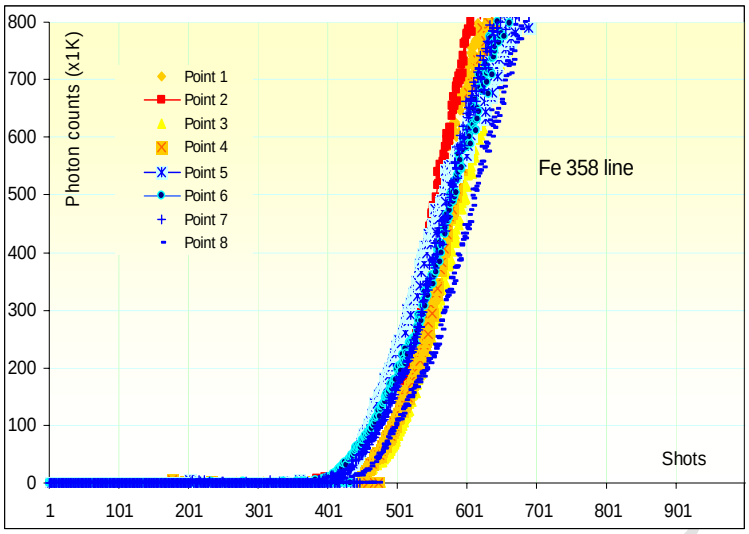

Figure 6: Consistency of the Fe 358.1 *nm* spectral line intensity for eight different spots along a semicircle, having constant radius (3 *mm*) from the coin center

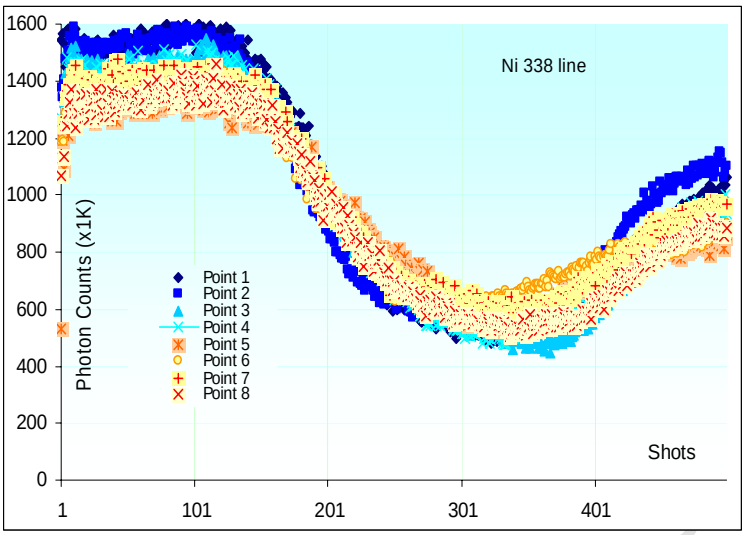

Figure 7: Consistency of the Ni 338.1 *nm* spectral line intensity for eight different spots along a semicircle, having constant radius (3 *mm*) from the coin center

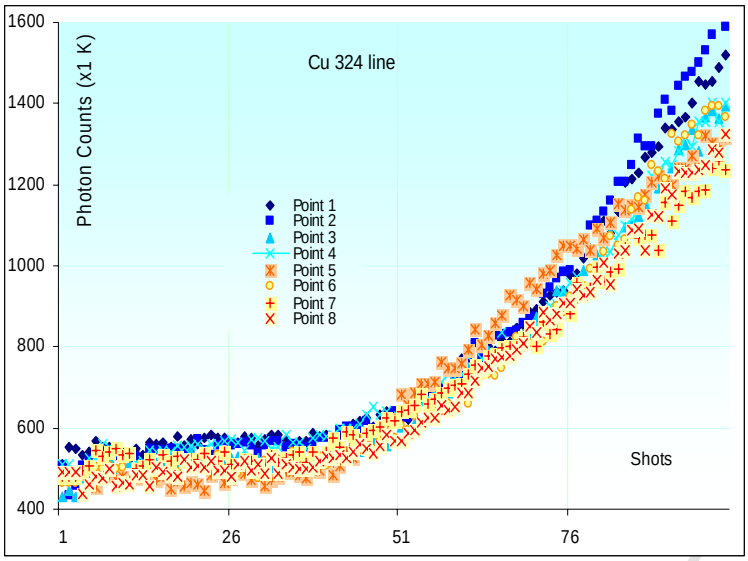

Figure 8: Consistency of the Cu 324.7 *nm* spectral line intensity for eight different spots along a semicircle, having constant radius (3 *mm*) from the coin center

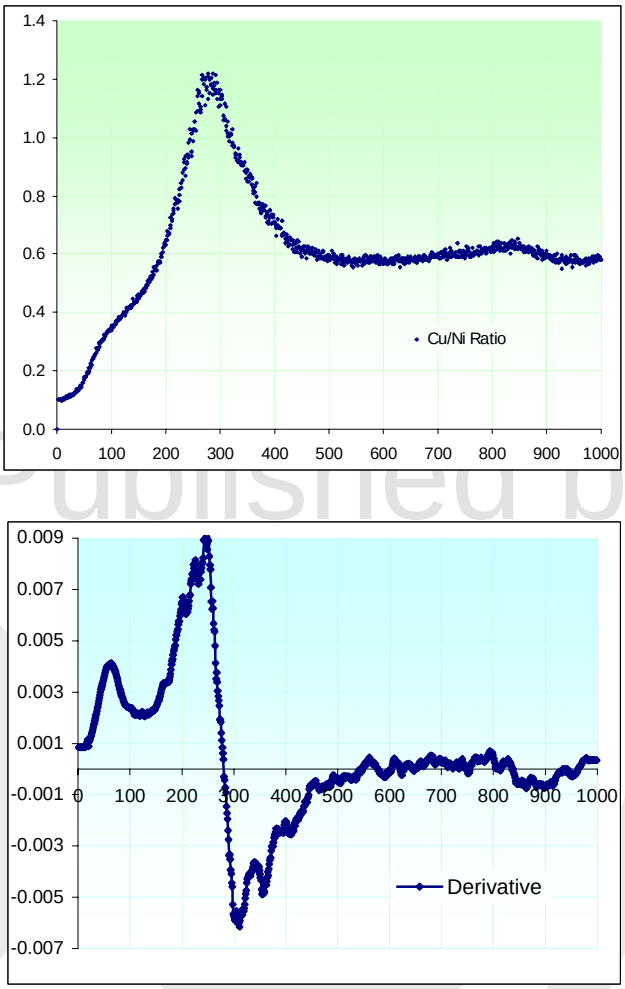

Figure 9: (a) Cu/Ni line intensity ratio and (b) Derivative. Zero crossing indicates transition from Cu to Ni.

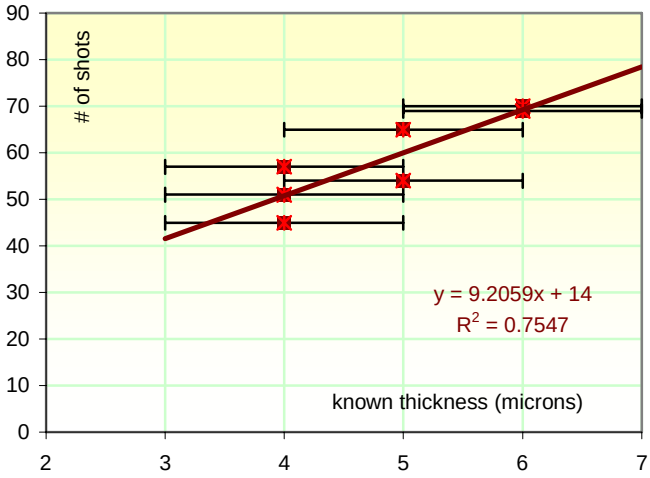

Figure 10: Seven-point interface A (Ni-Cu) calibration curve.

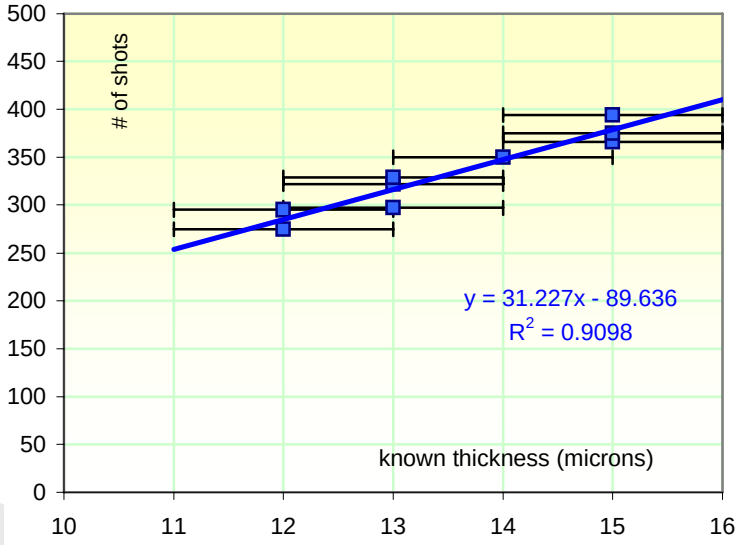

Figure 11: Nine-point interface B (Cu-Ni) calibration curve.

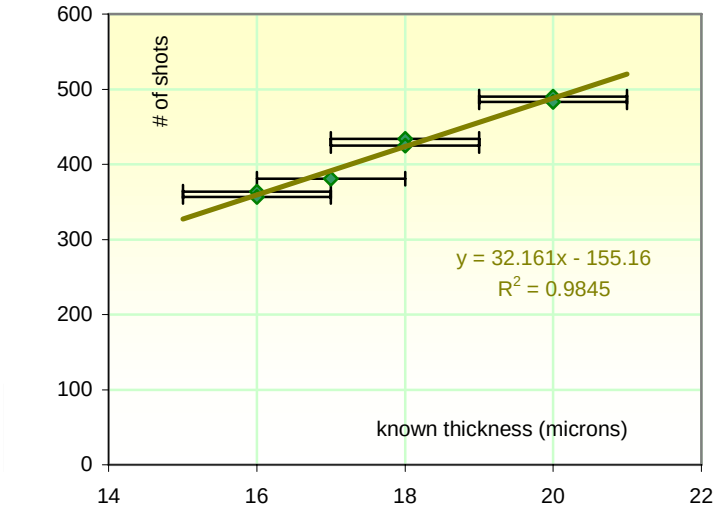

Figure 12: Seven-point interface C calibration curve.